How shear helps lava to flow

A. Harris, S. Mannini, S. Thivet, Magdalena Oryaëlle Chevrel, Lucia Gurioli, N. Villeneuve, A. Di Muro, Aline Peltier

How shear helps lava to flow

A. Harris[1], S. Mannini[1*], S. Thivet[1], M.O. Chevrel[1], L. Gurioli[1], N. Villeneuve[2], A. di Muro[2], A. Peltier[2]

[1]Université Clermont Auvergne, CNRS, IRD, OPGC, LMV, F-63000 Clermont-Ferrand, France

[2]OVPF, Institut de Physique du Globe de Paris, Sorbonne Paris Cité, Univ. Paris Diderot, CNRS, F-97418, La Plaine des Cafres, La Réunion, France

**Now at: University of Geneva*

ABSTRACT

Understanding the thermo-rheological regime and physical character of lava while it is flowing is crucial if we are to adequately model lava flow emplacement dynamics. We present measurements from simultaneous sampling and thermal imaging across the full width of an active channel at Piton de la Fournaise (La Réunion, France). Our data set involves measurements of flow dynamics at three sites down-channel from the vent. Quantification of flow velocities, cooling rates, sample texture and rheology allows all thermo-rheological parameters to be linked, and down- as well as cross-channel variations to be examined. Within 150 m from the vent we recorded an unexpected velocity increase (from 0.07 to 0.1 m/s), in spite of cooling rates of 0.19 to 0.29 °C/m and constant slope. This change requires a switch from a Newtonian-dominated regime to a Bingham plug-dominated regime. Sample analysis reveals that the plug comprises foam-like lava and the shear zones involve vesicle-poor (low viscosity) lava. With distance from the vent, shear zones develop carrying the vesicular plug between them. This causes flow to initially accelerate, helped by bubble shearing in narrow lateral shear zones, until cooling takes over as the main driver for viscosity increase and, hence, velocity decrease.

Key words: Lava channel; Velocity; Cooling; Vesicles; Viscosity; Shearing.

INTRODUCTION

Understanding the thermo-rheological regime of an active lava is fundamental if we are to adequately model its emplacement behavior (e.g., Harris and Rowland 2001; Hidaka et al. 2005; Del Negro et al. 2005). The interrelation between flow physical properties and dynamics is a crucial link for which we are rich in heat-loss-driven models (e.g., Keszthelyi and Self 1998), but lacking in data to allow validation of models and theory. Traditionally, lava flow rheology has been modeled as a cooling-dominated process, so that the lava steadily cools, degasses and crystallizes down flow, increasing in viscosity from the vent to the flow front (e.g., Harris and Rowland 2001). However, to date only a few measurements have been performed to assess whether this assumption is valid, and these measurements have all been for active channels in Hawaii, with the first measurements being made more than a kilometer or two from the vent (Lipman and Banks 1987; Moore 1987; Crisp et al. 1994; Cashman et al. 1999). While such a down-channel thermal and rheological regime has been borne out by analysis of inactive channels (Soule et al. 2004; Riker et al. 2009; Chevrel et al. 2014, Robert et al. 2014; Rhéty et al. 2017), thermal measurements and modeling have also indicated that down flow cooling is inevitable and progressive, the rate depending on degree of insulation, flow velocity and channel dimensions (Harris and Rowland 2009). Other work has highlighted the importance of the crystallization sequence on lava viscosity and strain rate on influencing crystallization behavior and, hence, emplacement dynamics (e.g., Chevrel et al. 2014; Kolzenburg et al. 2018). The role of bubbles on lava transport properties is, however, very poorly constrained, and detailed measurements down near-vent segments of active channels are scarce, with Lipman and Banks (1987) remaining a precious resource.

Down-flow degassing will likely cause loss of volatiles and undercooling of the melt to trigger micro-crystallization, both of which will increase the viscosity of the lava mixture

(Sparks and Pinkerton 1978). Down-flow evolution of bubble quantity and shape may also affect rheology, where the mixture viscosity will decrease or increase depending on whether bubbles are deformed or not (Llewellin and Manga 2005). Down-flow degassing and loss of bubbles has also been documented in lava tubes (Cashman et al. 1994) and from the structure of inflated pāhoehoe flows (Cashman and Kauahikaua 1997), as well as from measurements along active (Cashman et al. 1999) and solidified (Riker et al. 2009) systems. The effect of vesicles on rheology has also been inferred from in-situ viscosity measurements on pāhoehoe lobes (Chevrel et al. 2018). However, no direct field measurements exist to constrain and link changing bubble states with flow dynamics down a lava channel.

Here, we present unique data from thermal imaging and sampling down the near-vent reach of an active lava channel at Piton de la Fournaise (Réunion Island, France) during July–August 2015. This allows simultaneous constraint and linking of down and across flow velocity, temperature and rheology. Surprisingly, we measure an acceleration within 150 m of the vent. At constant slope, this implies a down-flow evolution of the rheological regime (from Newtonian to Bingham) which is caused by strain localization on the margin of a central plug. This can be supported by the difference in bubble content between lava sampled in the plug and shear zones. Our current understanding of lava flow is that it can evolve from Newtonian to Bingham rheology, but bubbles are rarely taken into consideration to explain such evolution. Here, we provide a unique data set that documents this evolution and attempt to model this with available rheological models (as detailed in the supplements), showing that bubbles play a fundamental role in determining rheology and evolving flow dynamics.

MEASUREMENTS IN AN ACTIVE LAVA CHANNEL

Channel dimensions and surface velocity

Piton de la Fournaise's July–August 2015 eruption lasted two days (31 July–1 August) and fed a single master channel which extended 1 km (Supplement 1). Down this stable channel

system thermal image sequences were collected at four stations (30, 110, 220 and 440 m from the vent, Fig. 1) on the same day (1 August) and within 20 minutes of each other (Supplement 2). Using manual particle tracking (Supplement 2) surface velocities were measured at 0.03±0.01 m/s at the channel margins and 0.07±0.04 m/s at the center. The horizontal and vertical velocity profiles were best-fit with a parabolic equation (Supplement 2), indicating horizontal velocity gradients of 0.07 s^{-1} (Fig. 2) and suggesting that flow was laminar and Newtonian. Further down flow (at stations 2 and 3, Fig 1), the channel was wider (4-5 m, instead of 2 m) and shallower (0.8 m instead of 1.8 m, Supplement 2). A constant surface velocity was measured across a central, 3 m-wide, plug at an average of 0.1 m/s at both stations, which was faster than at station 1 (Fig. 2). The central plug was flanked by two narrow, 0.5 m-wide, shear zones where velocity declined to zero (Fig. 2a). These profiles revealed a plug-dominated Bingham behavior, with a velocity gradient across the shear zones of 0.2 s^{-1}; a rate three times higher than at station 1. Assuming that the plug comprises 75% of the flow by thickness (as it does by width), then the plug height was 0.47 m, for a basal shear zone height of 0.16 m, across which the velocity vertical gradient was 0.45 s^{-1} (Fig. 2b).

Heat loss and cooling rate

Eruption temperature at the vent (1146 °C) was obtained from thermal images of bubbles bursting at the vent. At station 1 flow was poorly crusted, with a mean surface temperature of 704±107 °C (Supplement 3). At stations 2 and 3, while the surface of the central plug was partially covered by a crust of fragmenting slabs of spiny pāhoehoe and nascent ’a’ā, the shear zones had a cover of down-flow thickening ’a’ā. Due to the crust cover of the shear zones, surface temperatures at the channel margins were cooler than at the center, where average surface temperatures of the plug was 558±38 °C, but 300 °C at the margin (Fig. 3). These surface temperature ranges converted to heat losses of 87±2 kW/m^2 at station 1, and 31±24 and 45±23 kW/m^2 at stations 2 and 3. Cooling was then estimated between the vent and at

101 station 1 at 0.21±0.07 °C/m. Lower heat losses and higher velocities at stations 2–3 resulted in
102 cooling of 0.13±0.10 and 0.12±0.10 °C/m, at the two stations, respectively (Supplement 3).
103 Such cooling per unit distance is high in comparison to previously reported values for flow
104 down a lava channel (typically 0.005–0.007 °C/m, Crisp et al. 1994; Cashman et al., 1999;
105 Soule et al. 2004; Riker et al. 2009; Robert et al. 2014; Rhéty et al. 2017). This is because, for
106 our channel, lava was poorly insulated and velocities were low.
107
108 **Sampling, sample characteristics and lava viscosity**
109 Lava was sampled on the first day near the vent and on the second day at Station 2 coincident
110 with thermal imaging (Supplement 4). The station 2 sample was collected by inserting a metal
111 rod laterally 50 cm into the channel resulting in two distinct, simultaneously collected,
112 fragments: one from the shear zone and one from the plug. Mass flux was steady during field
113 work of day 2, during which this key (shear zone and plug) sample was collected coincident
114 with the thermal imagery.
115 Lava bulk composition was basaltic with a porphyritic texture (<3 vol.% phenocrysts;
116 15-34 vol. % microlites of plagioclase and pyroxene; Supplement 4). Near-vent samples had a
117 bulk density of 1370±280 kg/m^3, resulting in a vesicularity of 53±10 vol.%. Vesicles were
118 rounded with equivalent diameters of 1 mm (Fig. 4). Temperature estimated from the glass
119 MgO content was 1138±2°C (Supplement 4). The two station 2 sample fragments had
120 contrasting textural characteristics. The shear zone part was dense (2020 kg/m^3) with a
121 vesicularity of 30 vol.%, including rounded and small (0.5 mm) vesicles and a few larger (>2
122 mm) vesicles. Crystals showed alignment and the calculated melt temperature was 1119±1
123 °C. The difference between melt temperature near the vent and of the sample from the shear
124 zone resulted in a cooling per unit distance of 0.17 °C/m which agrees with the theoretical
125 calculations obtained from heat loss (Supplement 3). Conversely, the central plug fragment

had an extremely low density (500 kg/m^3), a very-high vesicularity (83 vol.%) and crystals were the less abundant (17 vol.%). The vesicle population was heterogeneous being a mixture of small-rounded (10–100 μm), larger-rounded (< 0.5 mm) and irregularly-shaped vesicles.

At station 1, the strain rates were relatively low (0.07 s^{-1}) and the bubble capillary number (Ca) was around 0.7 (Supplement 4). Given a threshold Ca of 0.5, above which bubbles are able to deform (Manga et al. 1998), i.e. bubble internal forces are weaker than the surrounding fluid forces (viscosity×strain-rate), the apparent viscosity of the three-phase lava (i.e. melt+crystal+bubbles) was estimated at 1.5×10^3 Pa s (Supplement 4). At station 2 within the shear zones the vesicle-free (melt+crystal) viscosity was higher at 8.4×10^3 Pa s due to lower temperature. However, because strain rates were 0.2 s^{-1} in the plug and 0.45 s^{-1} in the shear zones, we obtained Ca>>0.5 in these locations—meaning that bubbles were highly deformable. The effect of the bubbles therefore decreased the effective viscosity to 4.7×10^3 Pa s. Conversely, within the plug, although crystallinity was lower, the very high bubble concentration (>80 vol. %) and very low strain rates (near 0 s^{-1}) prevented bubbles deformation.

DISCUSSION

Given the interior flow temperature difference of 19 °C between stations 1 and 2, an average surface velocity of 0.05 m/s at station 1 and a distance between the two stations of 80 m, the time to travel to station 2 was around 1600 s. This gives cooling along the shear zones at a rate of ~0.012°C/s, which is in line with cooling rates obtained for active flows in Hawaii (Cashman et al., 1999). Given such a decrease in temperature we would expect a viscosity increase, and hence velocity decrease, down this vent-proximal channel length. However, the measured velocities revealed an acceleration between stations 1 and 2, after which velocity was constant until station 3. Given a constant slope between the three stations and stable effusion rate at the time of measurements, we explain this as a change in rheological behavior

by strain localization on either side of a down-flow-developing central plug (i.e., within the shear zones).

We therefore propose a scenario whereby lava emitted at the vent flowed under a Newtonian regime, as supported by the parabolic velocity profile. After 110 m (by station 2), narrow shear zones had appeared either side of a central plug, suggesting that flow had become Bingham. In the central plug, high bubble concentration and low strain rates resulted in bubble growth and increasing capillary forces resulting in a polyhedral foam with internal yield strength and stabile bubble walls so that the plug was not flowing. Instead it behaved as a solid, being carried between the two marginal shear zones. At the channel margins, although temperature was lower than near the vent, strain rates were so high that bubbles were sheared. The effect of this sheared-bubble population on flow bulk rheological properties outweighed the effect of cooling, resulting in a lower viscosity. The non-sheared and bubble-rich plug was thus carried between two lateral zones of sheared lava, highlighting the effect of bubbles which either acted as a lubricant in the shear zones or as a retardant to deformation in the plug. We note, also, that that the shear zone had lower MgO than the plug (Supplement 4). This could be due to preferential settling of larger olivine crystals in the slower moving shear zones, further supporting the fact that the shear and plug zones were independent identities.

The lower bubble content within the shear zones could be due to more outgassing than in the plug, or shear pressing of bubbles out of the marginal shear zones and into the central plug. However, due to relaxation effects during the time between sampling and quenching (Moitra et al. 2013; Lindoo et al. 2017), the evidence of the shearing effect is lost from the vesicle signature, but is visible from microlite alignment (Fig. 4b).

The change in flow regime over the proximal reach of the flow, from shear dominated with a parabolic velocity profile at the vent to plug dominated after 110 m is reflected in the temperature profiles (Fig. 3). Temperatures are high across the entire channel near-vent

because of a highly disrupted, young crust. At stations 2 and 3, temperatures become low in the marginal shear zones where an increasingly thick carapace of mature ’a’ā is built (cf. Rowland and Walker, 1987), and higher across the central plug where slabs of crust can form, which then broke-up to expose hotter interior lava. The lower velocities of the shear zone lava also meant that lava at the channel margins had more time to cool and develop a more mature crust than at the center, as well as giving time for larger olivines to preferentially settle and gas to escape.

CONCLUSION

An unexpected velocity increase and apparent viscosity decrease was recorded down a lava channel over the first 110 m of flow, in spite of stable slope, constant mass flux and high cooling rates. This peculiar change was caused by the down-flow development of a central plug flanked by narrow shear zones in which bubbles were highly deformed; and hence where the effective viscosity is low. As in a volcanic conduit (e.g., Wright and Weinberg 2009), the lateral shear zones lubricate the central plug. This causes the flow to initially accelerate over the proximal reach of the channel until cooling and crystallization can take over as the main drivers for viscosity increase and, hence, velocity decrease.

Our measurements represent a unique (and difficult to obtain) near-vent data set (given here in the data repository and fully described in the supplement) in which, for the first time, we can identify and quantify a velocity increase over a relatively short distance close to the vent. Future measurements will need to focus on this near-vent part of the channel system so as to properly define and explain the complete down-channel evolution of flow dynamics, and add to this repository.

ACKNOWLEDGMENTS

This work was funded by the Agence National de la Recherche through project ANR-LAVA (ANR Program: DS0902 2016; Project: ANR-16CE39-0009) and greatly benefitted from the

constructive comments of two anonymous and three named (Matthew Patrick, Einat Lev and Kathy Cashman) reviewers. This is ANR-LAVA contribution no. X.

REFERENCES CITED

Cashman, K V, C Thornber, and J P Kauahikaua. 1999. "Cooling and Crystallization of Lava in Open Channels, and the Transition of Pāhoehoe Lava to 'a'Ā." *Bulletin of Volcanology* 61: 306–23. doi:https://doi.org/10.1007/s004450050299.

Crisp, J, K v. Cashman, J A Bonini, S B Hougen, and D C Pieri. 1994. "Crystallization History of the 1984 Mauna Loa Lava Flow." *Journal of Geophysical Research* 99 (B4): 7177–98. doi:10.1029/93JB02973.

Harris, A. J. L., John Bailey, Sonia Calvari, and Jon Dehn. 2005. "Heat Loss Measured at a Lava Channel and Its Implications for Down-Channel Cooling and Rheology." *Geological Society of America Special Papers* 396 (09): 125–46. doi:10.1130/2005.2396(09).

Harris, A J L, and S K Rowland. 2001. "FLOWGO: A Kinematic Thermo-Rheological Model for Lava Flowing in a Channel." *Bulletin of Volcanology* 63: 20–44. doi:10.1007/s004450000120.

———. 2009. "Effusion Rate Controls on Lava Flow Length and the Role of Heat Loss: A Review." *The Legacy of George P.L. Walker, Special Publications of IAVCEI. Eds Hoskuldsson A, Thordarson T, Larsen G, Self S, Rowland S. Geological Society, London.* 2: 33–51.

Hidaka, M, A Goto, S Umino, and E Fujita. 2005. "VTFS Project: Development of the Lava Flow Simulation Code LavaSIM with a Model for Three-Dimensional Convection, Spreading, and Solidification." *Geochemistry, Geophysics, Geosystems* 6: Q07008.

Keszthelyi, L, and S Self. 1998. "Some Physical Requirements for the Emplacement of Long Basaltic Lava Flows." *J. Geophys. Res.* B11: 27,447-27,464.

226 Kolzenburg, S., D. Giordano, K-U. Hess, and D.B. Dingwell. 2018. “Shear-rate Dependent
227 Disequilibrium Rheology and Dynamics of Basalt Solidification.” *Geophysical Research*
228 *Letters*. doi:doi.org/10.1029/2018GL077799.
229 Lipman, P W, and N G Banks. 1987. “Aa Flow Dynamics, Mauna Loa 1984.” *U.S. Geol.*
230 *Surv. Prof. Pap 1350*, 1527–67.
231 Llewellin, E W, and M Manga. 2005. “Bubble Suspension Rheology and Implications for
232 Conduit Flow.” *Journal of Volcanology and Geothermal Research* 143: 205–17.
233 Moore, H J. 1987. “Preliminary Estimates of the Rheological Properties of 1984 Mauna Loa
234 Lava.” *U.S. Geological Survey Professional Paper 1350* 99: 1569–88.
235 Negro, C Del, L Fortuna, A Vicari, C Del Negro, L Fortuna, A Vicari Modelling, and
236 Nonlinear Networks. 2005. “Modelling Lava Flows by Cellular Nonlinear Networks
237 (CNN): Preliminary Results.” *Nonlinear Processes in Geophysics* 12: 505–13.
238 Rhéty, M., A. J. L. Harris, N. Villeneuve, L. Gurioli, E. Médard, M.O. Chevrel, and P.
239 Bachèlery. 2017. “A Comparison of Cooling-Limited and Volume-Limited Flow
240 Systems: Examples from Channels in the Piton de La Fournaise April 2007 Lava-Flow
241 Field.” *Geochemistry, Geophysics, Geosystems* 18 (9): 3270–91.
242 doi:10.1002/2017GC006839.
243 Riker, J M, K V Cashman, J P Kauahikaua, and C M Montierth. 2009. “The Length of
244 Channelised Lava Flows: Insight from the 1859 Eruption of Mauna Loa Volcano,
245 Hawaii.” *Journal of Volcanology and Geothermal Research* 183: 139–56.
246 Robert, B, A Harris, G Gurioli, E Medard, A Sehlke, and A Whittington. 2014. “Textural and
247 Rheological Evolution of Basalt Flowing down a Lava Channel.” *Bulletin of*
248 *Volcanology* 76: 824.
249 Robertson, J. C., and R. C. Kerr. 2012. “Solidification Dynamics in Channeled Viscoplastic
250 Lava Flows.” *Journal of Geophysical Research: Solid Earth* 117 (7): 1–18.

doi:10.1029/2012JB009163.

Rowland, S.K., and G.P.L. Walker. 1987. "Toothpaste lava: characteristics and origin of a lava structural type transition between pahoehoe and ‘a‘a." *Bulletin of Volcanology* 49: 631-641

Soule, S. A., K.V. Cashman, and J. P. Kauahikaua. 2004. “Examining Flow Emplacement through the Surface Morphology of Three Rapidly Emplaced, Solidified Lava Flows, Kīlauea Volcano, Hawai’i.” *Bulletin of Volcanology* 66 (1): 1–14. doi:10.1007/s00445-003-0291-0.

Sparks, R S J, and H Pinkerton. 1978. “Effect of Degassing on Rheology of Basaltic Lava.” *Nature* 276: 385–86.

Wright, Heather M N, and Robert F. Weinberg. 2009. “Strain Localization in Vesicular Magma: Implications for Rheology and Fragmentation.” *Geology* 37 (11): 1023–26. doi:10.1130/G30199A.1.

FIGURE CAPTIONS

Figure 1. Map of the lava flow field (yellow outline), fissures (green outline), main vent (red outline) and stable channel (pink outline) of the July-August 2015 eruption of Piton de la Fournaise.

Figure 2. a) Mean (squares) and standard deviation (given as error bars) for all velocity measurements made. Lines are best-fit velocity profiles across the channel width at stations 1 (red), 2 (orange) and 3 (blue) using the approach of Supplement 2. b) Modeled vertical velocity profiles at stations 1 (red) and 3 (blue). For clarity, the mean and standard deviation of the total data set at the three stations is plotted and fitted here. Results are the same if we fit through individual measurement sample sets that make up the population that the mean describes, where (for any one measurement set) there is always a lower velocity at station 1 than at stations 2 and 3. The full data set, for each station, is described and plotted in Supplement 2. Note that the asymmetry of the measurements at stations 2 (S2) and 3 (S3) is due to the missing far bank shear zone, which we could not resolve from our low oblique viewing angle (see Supplement 2).

Figure 3. Surface temperature across the channel at stations 1 (red) and 3 (orange).

Figure 4. Binary images of the thin sections and back scattered electron images for (a) the near-vent sample of day 1, plus (b) the shear zone and (c) plug zone of the sample taken on day 2 (in the binary images white = matrix, grey = phenocrysts and black = vesicles).

N

Upper fissure

Main cone

1

2

3

4

Lower fissure

Flow direction

200 m

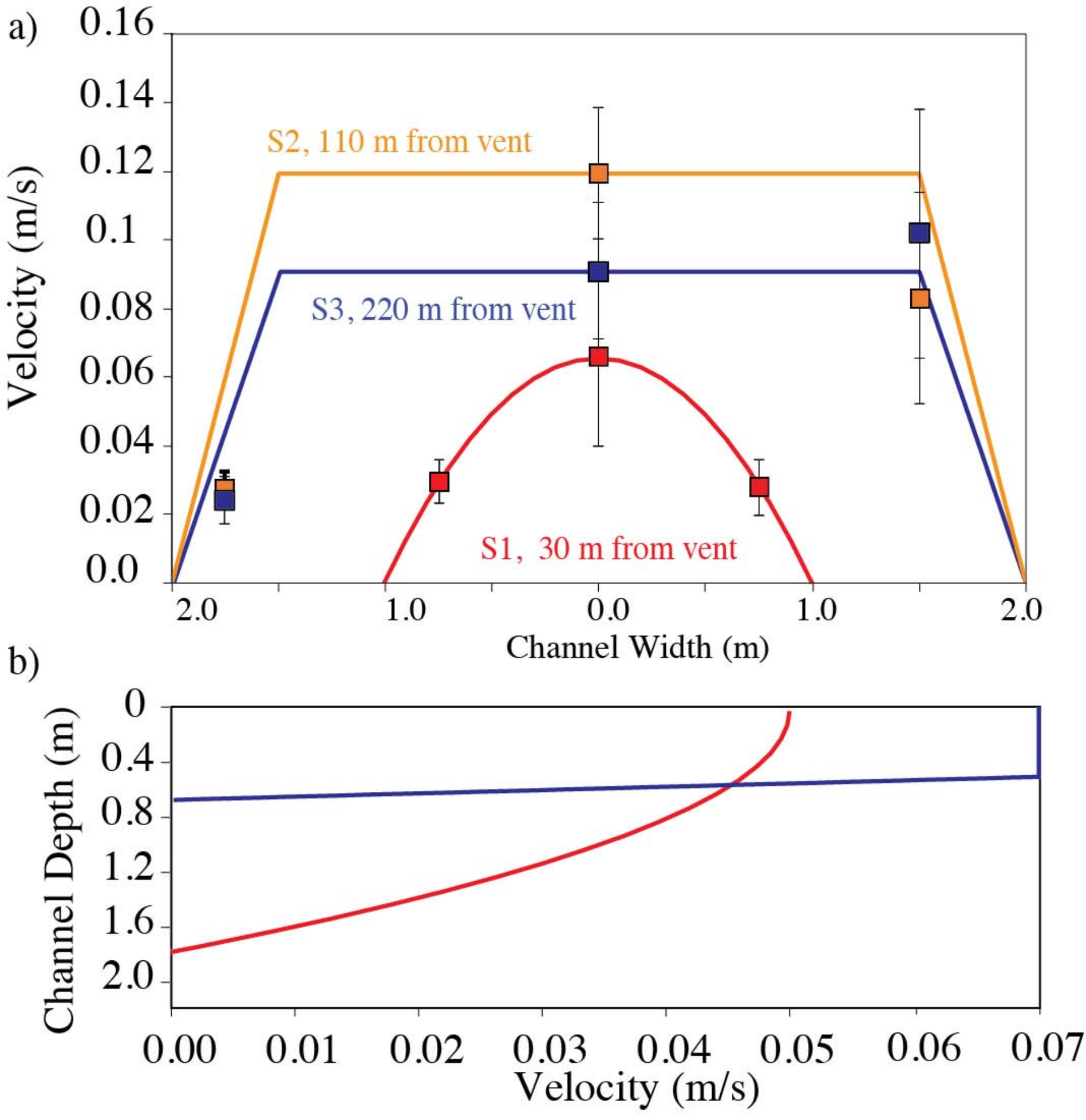
a)
0.16
0.14
0.12
0.1
0.08
0.06
0.04
0.02
0.0
Velocity (m/s)
S2, 110 m from vent
S3, 220 m from vent
S1, 30 m from vent
2.0
1.0
0.0
1.0
2.0
Channel Width (m)
b)
0
0.4
0.8
1.2
1.6
2.0
Channel Depth (m)
0.00
0.01
0.02
0.03
0.04
0.05
0.06
0.07
Velocity (m/s)

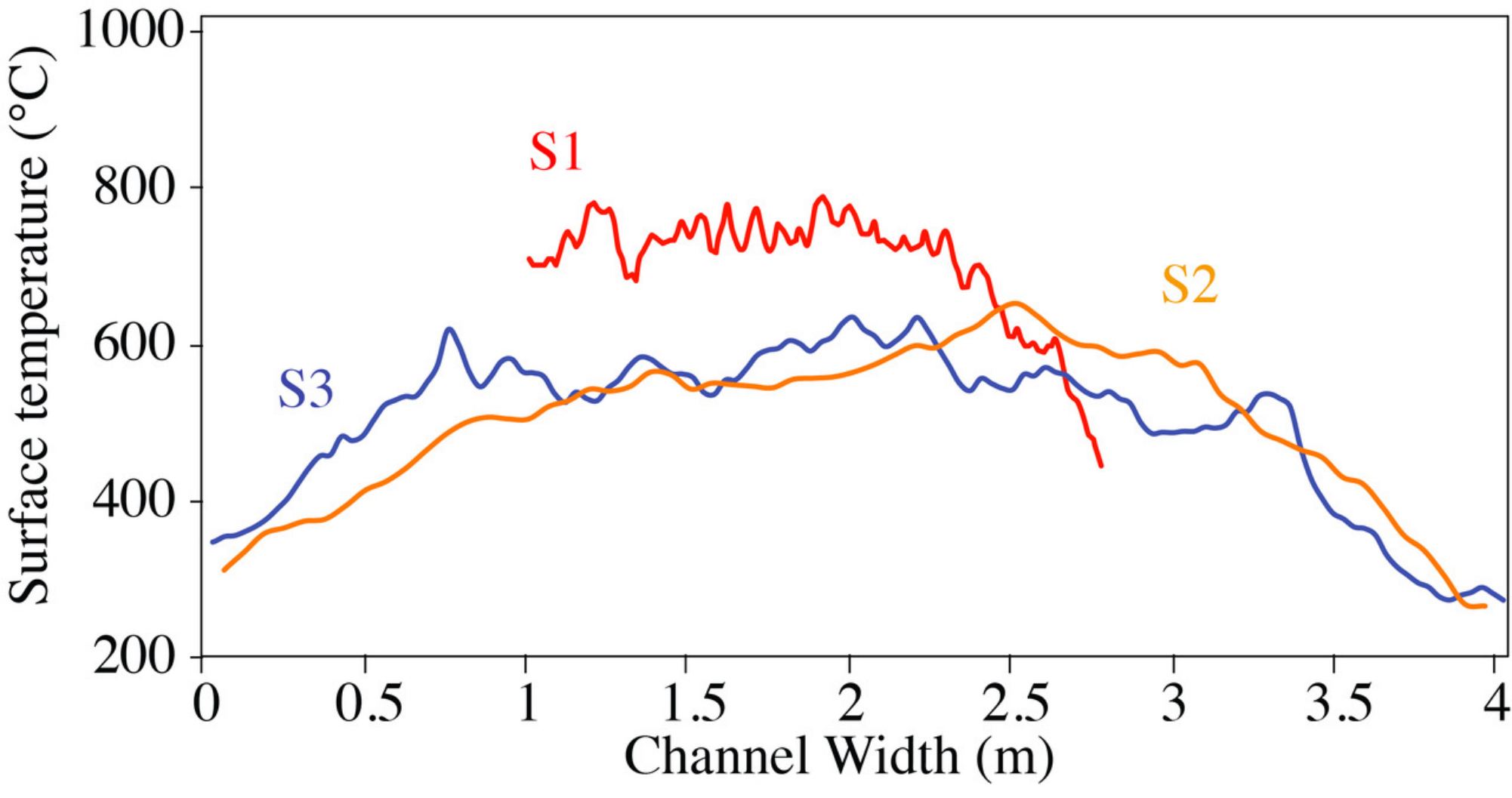
Surface temperature (°C)
1000
800
600
400
200
S1
S2
S3
0
0.5
1
1.5
2
2.5
3
3.5
4
Channel Width (m)

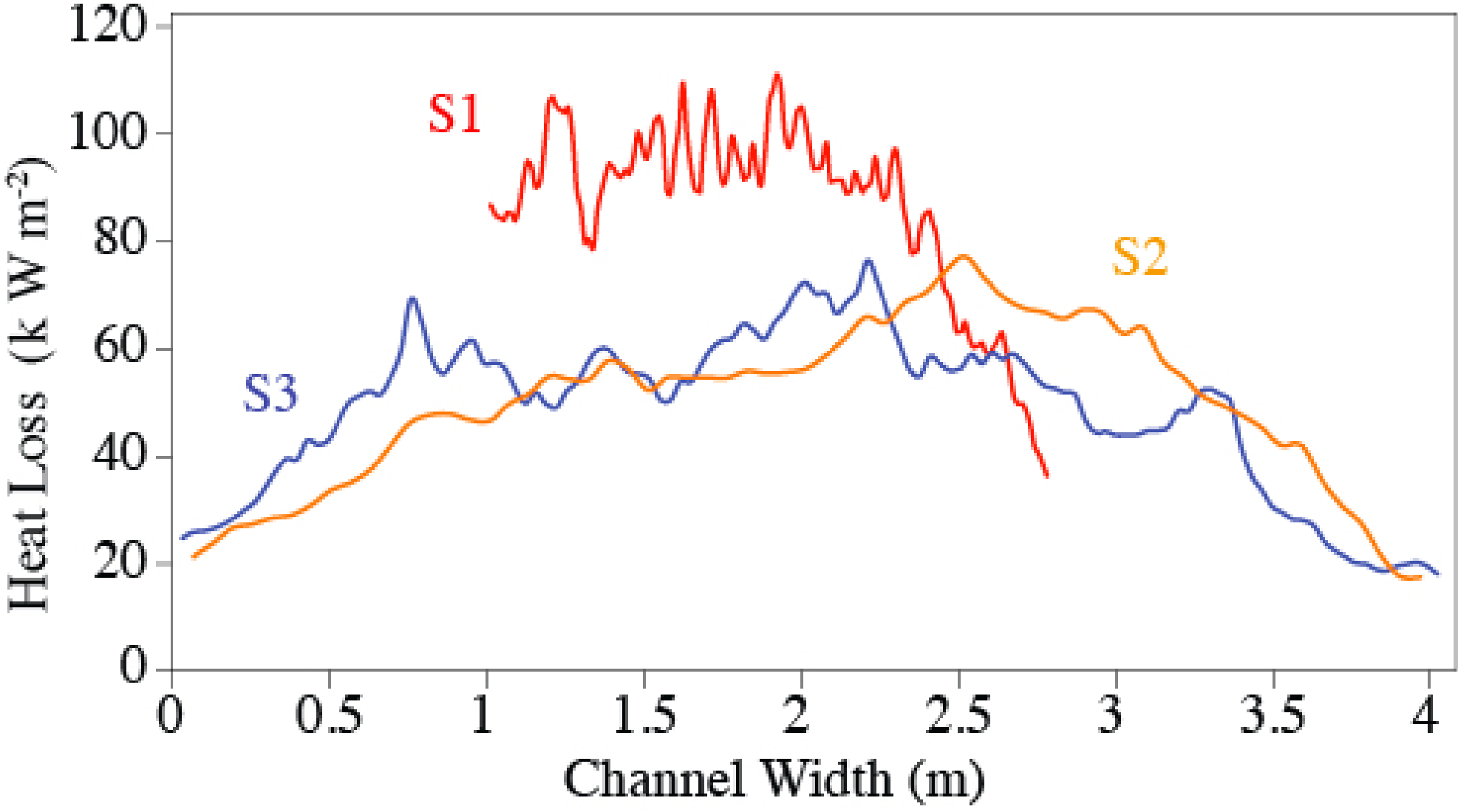
120
100
80
60
40
20
0
Heat Loss (k W m-2)
S1
S2
S3
0
0.5
1
1.5
2
2.5
3
3.5
4
Channel Width (m)

a) Example of sample near the vent

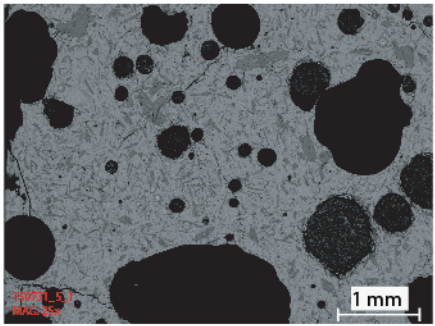

b) Shear zone s ample at Station 2

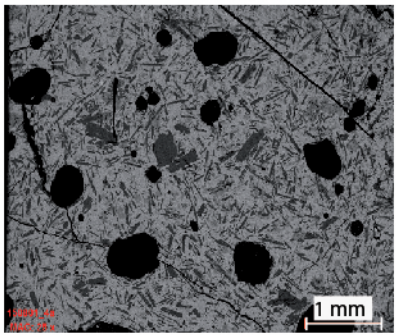

c) Sample from plug at Station 2